Latin American Journal of Solids and Structures
www.lajss.org

Numerical Modeling of Corrosion Effectson Ultimate Strength of DX Tubular Joints

Abstract

This article presents the results of numerical investigation on modeling buckling behavior and ultimate strength of corroded multi-planar tubular joints. Finite element method was used in order to simulate the behavior of DX multi-planar tubular joints under axial compressive loading.

Three different patterns were chosen for corrosion modeling. Also the effects of corrosion-related parameters such as age and depth of corrosion were evaluated. The first corrosion pattern is based on uniform reduction of wall thickness over a portion of tube length while the second pattern represents a sinusoidal reduction of thickness. The third pattern of corrosion uses average thickness and standard deviation as main parameters for defining a random corroded region. A linear criterion for predicting corrosion wastage has been used for the first and the second patterns, whereas predictions of the third pattern are determined by a nonlinear method.

The results indicate differences in the ultimate strength concluded from different patterns. It was found that conventional methods are conservative in evaluating the strength of corroded tubular joints of jacket platforms. Amongst 3 methods used for modeling corrosion, the third and the second pattern had similar results. It was also shown that corrosion is ineffective in braces and increasing the number of waves for the second pattern will result in increase of joint strength.

The optimum sizes of elements were defined by implementing an analysis of model sensitivity toward element size.

Keywords

Multi-planar tubular joints, DX joints, corrosion, Finite Element Method (FEM), ultimate strength, jacket platform.

Majid Rashidi [a]
Masoud Nazari [a]
Mohammad Reza Khedmati [a,*]
Akbar Esfandiari [a]

[a] Department of Maritime Engineering, Amirkabir University of Technology, 424 Hafez Avenue, Tehran 15916-34311, Iran

*Author email: khedmati@aut.ac.ir

http://dx.doi.org/10.1590/1679-78253118

Received 25.05.2016
In revised form 12.11.2016
Accepted 16.11.2016
Available online 29.11.2016

1 INTRODUCTION

Introduction of modern methods for petroleum extraction and economic benefits of using old platforms result in utilizing platforms beyond their design service lives. Therefore, for the purpose of safety and maintenance of a platform, it is necessary to investigate the remaining strength of corroded joints. Corrosion is a time-dependent electrochemical process and depends on the circumstances surrounding the structure. It should be noted that corrosion is occurs in the form of galvanic type in the sea environment (Cosham *et al.* (2007)). Corrosion is usually divided into two main groups: general and localized corrosion. In case of tubular members, especially in the sea, the definition is different. According to Hairil Mohd and Paik (2013), the corrosion definition in terms of the extent of the corrode area is divided into 5 groups of ring, line, general, limited and hole corrosion. Each corrosion type affects a specific area of the tube. The dimensions of damaged area can be expressed by multiples of tube diameter (D) in circumferential and longitudinal direction of the tube. Figure 1 shows corroded area dimensions for 5 corrosion types.

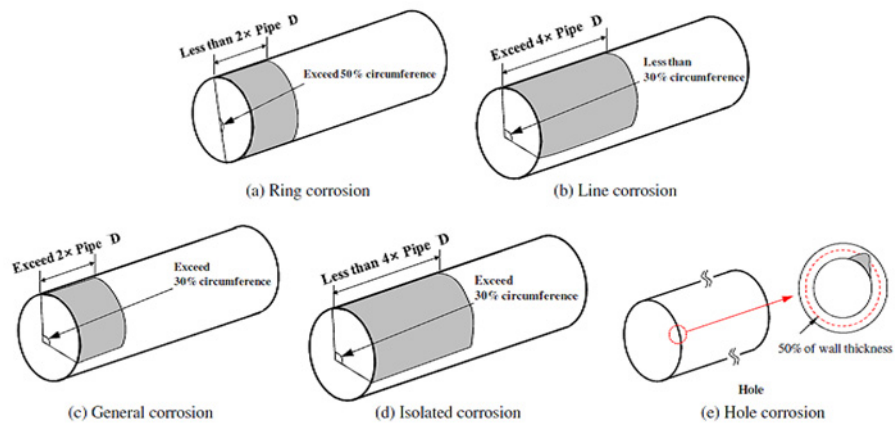

Figure 1: Different corrosion types and development of damaged area over the surface of tubular members (Hairil Mohd and Paik (2013)).

There are many factors affecting the speed of corrosion propagation, e.g. polarity of the metal, temperature, water flow rate, pH of sea water and the location of structure (Chamberlain (1988) and Wika (2012)).There is not a comprehensive research performed on ultimate strength of corroded joints and in general it is suggested that the designer should consider 10-12 mm (if no anti-corrosion coating is included) to compensate reduction of corrosion thickness for tubular members (UEG offshore Research (1985).In jacket platform, tubular joints play an important role in load bearing and structural strength. As important structural elements, the study of static strength gives an overall prospect of entire structure.

Tubular joints are considered as the weakest points of an offshore structure. Some researchers showed that failures begin from joints e.g. Lesani et al (2013). The studies on tubular joints are mainly concentrated on fatigue, stress concentration factors (SCF) and static strength of joints.

Numerical models and empirical formulas were used in these issues for different joints. Researches in the field of tubular joints can be categorized into three main groups, i.e. experimental, numerical and analytical studies. Empirical studies began in the 60s by Togo *et al.* (1967) and Washio *et al.*(1968-69). Among the most important researches, Chiew *et al.* (1997) performed a test on a DX joint to obtain its ultimate strength (Figure 2). The test conditions were similar to the real conditions and a full scale model was used. In this test the ultimate static strength of the joint was studied under compressive loading of bracing members, so that 350 kN was first applied to the out of plane braces and then 400 kN was applied to the in-plane braces. Afterwards the loading was only applied to in-plane braces and increased in controlled manner until the plastic deformation of the chord occurred.

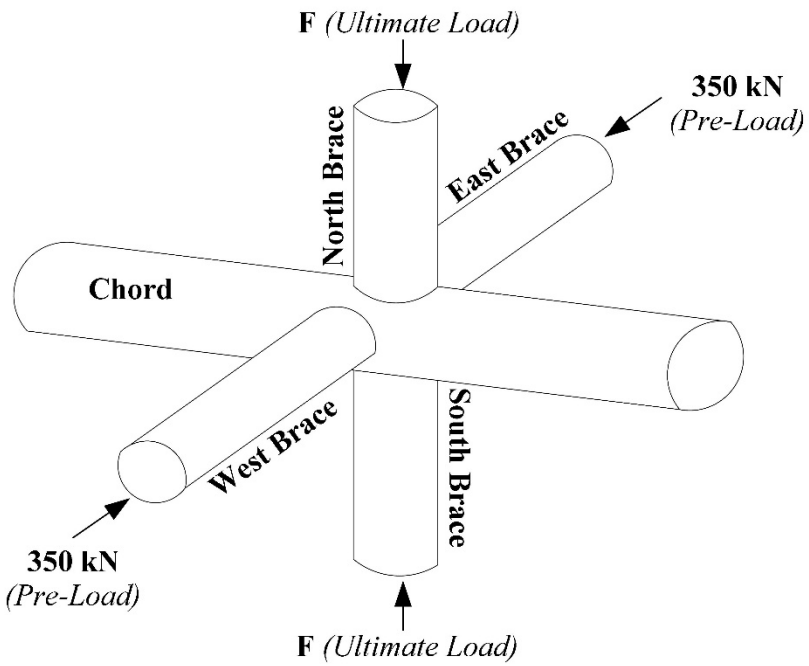

Figure 2: 3 steps of loading for a DX joint (Chiew *et al.* (1997)).

Gho *et al.* (2006) studied on K overlapped joints with a concentration on stress and joint failure mechanism. They concluded that the empirical formulas are conservative to estimate the stress concentration factor in many cases. They used 8-node shell elements of MARC and MENTAT software in order to investigate stress concentration factor of K joints. Chen *et al.* (2016) performed a numerical study on strength of tubular X-joints reinforced by grouting. Studying the results of the PATRAN, FEMGEN and ANSYS software on K-shaped joint was conducted by Dexter (1996). He showed that ANSYS software is more efficient. The Static strength of collar plate and doubler plate reinforced tubular T/Y-joints was studied by Nassiraei *et al.* (2016). They derived formulas for determining strength of reinforced joints. Among the first researches in analytical field, Togo *et al.* (1967) studies can be noted that was based on the theory of plasticity. Their work was developed by Makelainen (1988) and Paul (1992). Three models of ring model, punching shear and chord

shear are used to determine tubular joint strength. Marshall *et al.* (1974) investigated joint strength using punching shear model. Lan *et al.* (2016) studied on internally ring-stiffened tubular DT-joints to obtain static strength formula and comparing them with numerical models.

A summary of researches in three groups of experimental, analytical and numerical studies for a variety of joints is depicted in Figure 3. As mentioned earlier, there is no investigation performed on the ultimate strength of joints with corrosion. Extensive researches have been carried out on strengthening of intact tubular joints; but there is a lack of knowledge on prediction of strength for aged structures. The reason is difficulties of analyzing corroded joint, especially for large experimental scales. Furthermore, complexities and novelties of corrosion modeling make it to be an untouched field of research.

In this paper a numerical method is used in order to determine the ultimate static strength of corrode DX joints. To do this, bracing member is loaded until the displacement-force curve reaches a maximum point (ultimate state).The validation of numerical model for non-corroded models is demonstrated for different kinds of loading conditions and boundary conditions.

The aims of this study can be listed as:

1. Modeling the thickness changes of the joint members using an efficient method that can effectively represent environmental conditions of the sea.
2. Obtaining the ultimate static strength of the corroded joint
3. Comparing the ultimate strength of the corroded joint with the intact joint.
4. Investigating the effects of basic parameters of corrosion patterns.
5. Predicting the ultimate strength of corroded joints as a function of time.

Researches Review		
Analytical	**Numerical**	**Experimental**
Togo (1967)	Yura (1987)	Togo:1967-69
Marshall (1974)	Dexter (1996)	Boone (1982)
Makelainen (1988)	Lee and Wilmshurst (1996-97)	Yura (1987)
Paul (1992)	Kang (1998)	van der Vegte (1991)
Lan (2016)	Chiew (1999)	**Moffat (1994)**
	Lee and Llewelyn-Parry (2005)	Chiew (1997)
	Gho (2006)	Kang (1998)
	Lesani (2013)	**Gho (2006)**
	Chen (2016)	Yang (2012)
	Nassiraei (2016)	Chen (2016)

Figure 3: Research overivew forstrength of tubular joints.

2 FINITE ELEMENT ANALYSIS

Due to complexities of stress distribution and load transmission mechanism for tubular joints, numerical methods are usually used to study behavior of tubular joints under different kinds of loading. In this study ANSYS 14 is used to conduct FE approach. The large deformation effects of numerical models involve nonlinearities of material and geometry. The material used has bilinear isotropic hardening properties. Accordingly, Von Mises yield criterion is introduced to Shell 181 elements. Figure 4 shows an FE model of a DX joint used in this study.

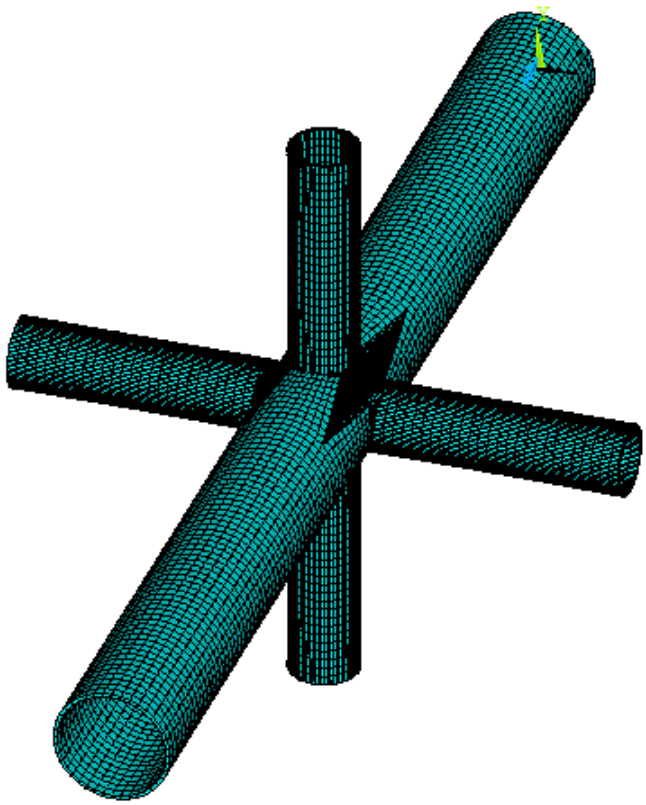

Figure 4: An isometric view of a FE model for DX joint

2.1 Joint Model

In this study, the DX multi-planar joints were modeled. The prepared models (without corrosion) were validated with boundary conditions according to two experiments, i.e. one-step loading (van der Vegte *et al.* (1991)) and 3-step loading (Chiew *et al.* (1997)). In order to obtain the appropriate meshing for corrosion modeling, the sensitivity of the models was assessed. In order to validate numerical models, the results were compared with those of other researchers, e.g. Chiew *et al.* and van der Vegte *et al.* The work of Chiew *et al.* provides more inclusive loading conditions as they studied in-plane and out of- plane loading of braces. Therefore it is better to compare the results with them; however, the results of van der Vegte *et al.* were also used for validation. The mechanical properties

are taken from Chiew *et al.* It should be noted that some joints with different geometrical properties have been modeled but due to writing restrictions they were not mentioned in this paper. The total number of models was 75, and only 20 models are discussed in thisstudy.

2.2 Boundary Conditions and Principles of Modeling

The boundary conditions used for models were same as the experiments. For one-step and 3-step loadings, according to the different laboratory conditions and type of materials, two different methods were used in applying boundary conditions.

2.2.1 One-Steploading

In this study the results of one step loading experiments performed by van der Vegte *et al.* (1991)are used. In other words, compression loading is applied to in-plane braces until the ultimate static strength is reached (Figure 5). According to Yura and Swenssen (1987), displacement control loading has been used.

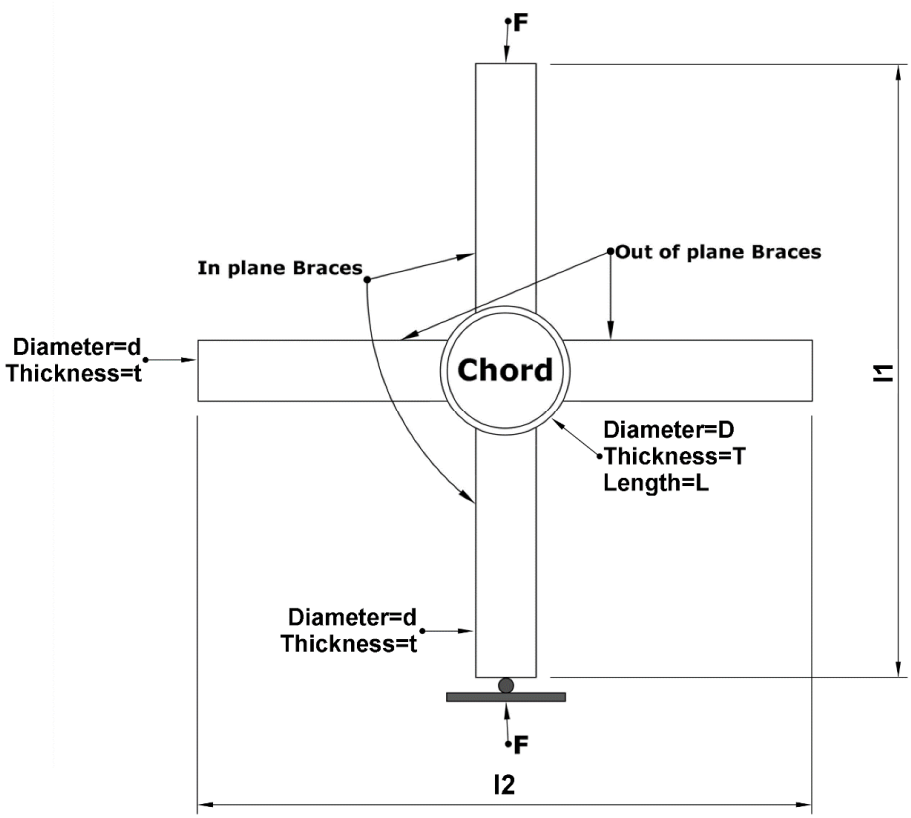

Figure 5: Loading condition in one-step loading test (van der Vegte *et al.* (1991)).

In this joint, steel with the standard of Euronorm 25 with 240 N/mm^2 yield stress has been used. Table 1 shows the geometry of this joint.

υ	σ_y (N/mm^2)	γ	τ	β	t(mm)	T(mm)	d(mm)	D(mm)	l2(mm)	l1(mm)	L(mm)
0.3	240	20	1	0.6	10	10	244.5	406.4	2856.4	2856.4	2440

Table 1: Geometrical and mechanical properties of the DX-joint for one-step loading test (van der Vegte *et al.* (1991)).

Where:

d=The outer diameter of the brace member,

D=The outer diameter of the main member (chord)

L=Length of the main member

t=Thickness of brace members

T= Thickness of main member

l1=Length of in-plane braces including the outer diameter of the main member

l2=Length of out of plane braces including the outer diameter of the main member

$\beta=\frac{d}{D}$ =Diameter ratio (indicating the density of the joint)

$\tau=\frac{t}{T}$ =Wall thickness ratio (indicating that the main member fails before the braces)

$\gamma=\frac{D}{2T}$ =Main member thickness parameter (indicating radial thickness and hardness of main member)

σ_y =Yield stress of steel

υ=Poisson's ratio

In this model, boundary conditions have been applied at the end of each member. In other words, 6 degrees of freedom for the elements at the end of members were constrained; only one axial translational degree of freedom is not fixed along of the member (Figure 6). The load-displacement curve for an experiment and the present FE model is shown in Figure 7.

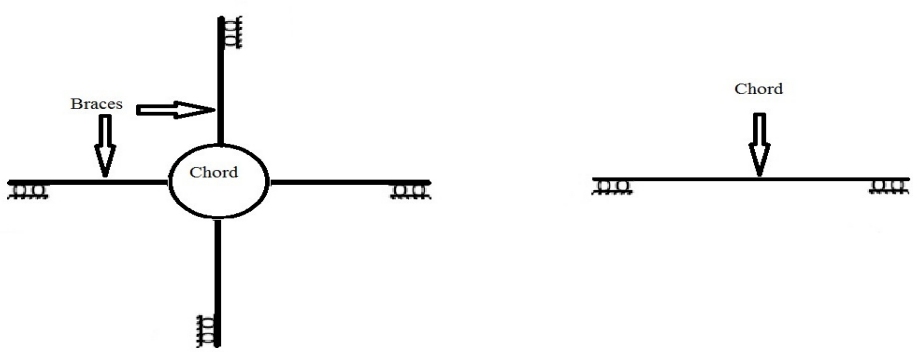

Figure 6: Boundary conditions for one-step loading model.

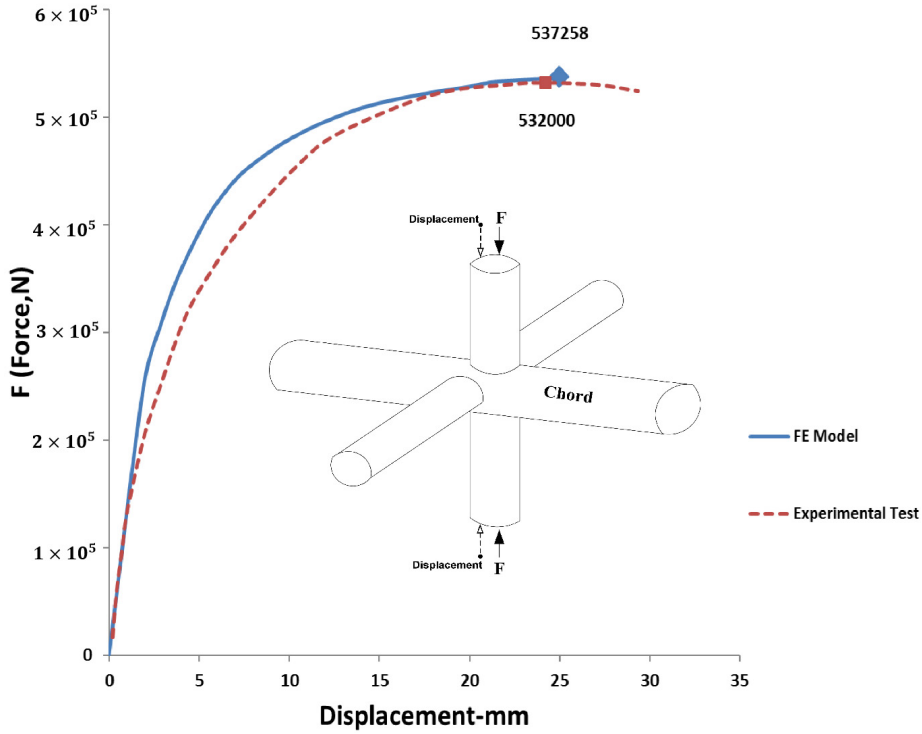

Figure 7: Finite element modeling result for one-step loading test (ultímate strength) (van der Vegte *et al.* (1991)).

2.2.2 3-Step Loading

The 3-step loading was used for analyzing corroded models. According to researches conducted, loading on bracings, $\alpha \geq 12$ coefficient(ratio of length multiplied by two to diameter of the main member) and support position of main member have no significant influence on the joint strength (Chiew *et al.* (1997)). This condition is the same as all corroded models. The procedure of loading is comprised of 3 different steps, i.e. at the first step, 350 kN compressive force is applied to the out of plane braces, then a force of 400 kN is applied to in-plane braces. Loading could change based on the joint capacity. Finally, a displacement controlled loading is applied on the joint until it fails (Chiew *et al.* (1997)). As previously mentioned, in these models bilinear isotopic hardening properties have been used. As seen in Figure 8, the material reaches the yield strength with a fixed slope (Young's modulus E). After yielding, plastic behavior is expressed by another slope, say E1. According to Khedmati research (2000), good value for E1 is E/65.

Table 2 presents mechanical properties of the material used in this stage, which is standard steel API 5L Grade B with yield stress of 361.8 N/mm^2. As shown in Figure 8, the hardening curve is similar to one-step, but it is different in the amount of E and E1. In this model the variables have been changed based on research of Miki *et al.* (2000). It should be noted that after applying the preload force, in-plane braces moves upward that is opposite the compressive force exerted on the braces in the next loading step. In other words, the geometry of numerical model should be updated for the next load steps.

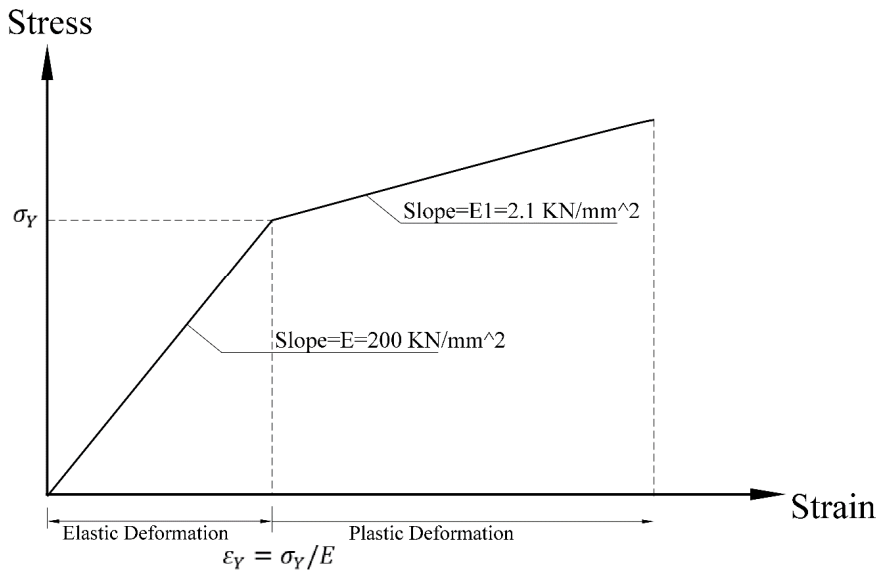

Figure 8: Stress-strain curve for 3-step loading.

υ	σ_y (N/mm^2)	γ	τ	β	t(mm)	T(mm)	d(mm)	D(mm)	l2(mm)	l1(mm)	L(mm)
0.3	361.8	24.5	0.98	0.6	9.1	9.3	273.05	457.2	3079.2	2951.2	4997.2

Table 2: Geometrical and mechanical properties of DX-joint in 3-steps loading test (Chiew *et al.* (1997)).

The boundary conditions are the same as one step loading models with the exception that from 6 degrees of freedom only 2 degrees of freedom for lateral translational is fixed (Figure 9). Figure 10 depicts the curves of load-displacement for an experiment and the present FE model. The ultimate strength obtained by numerical model differs from experimental results by about 3.9%. Also, the numerical force-displacement graph matches well with the experiment curve. The results of these two models (one-step and 3-step) indicate that the numerical models of DX tubular joints used in this study are reliable.

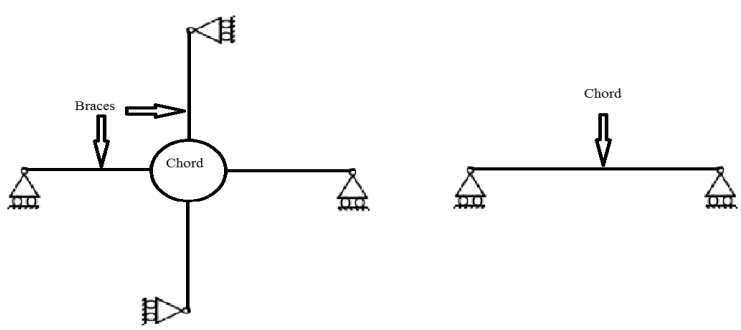

Figure 9: Boundary condition in FE modeling for 3-step loading test.

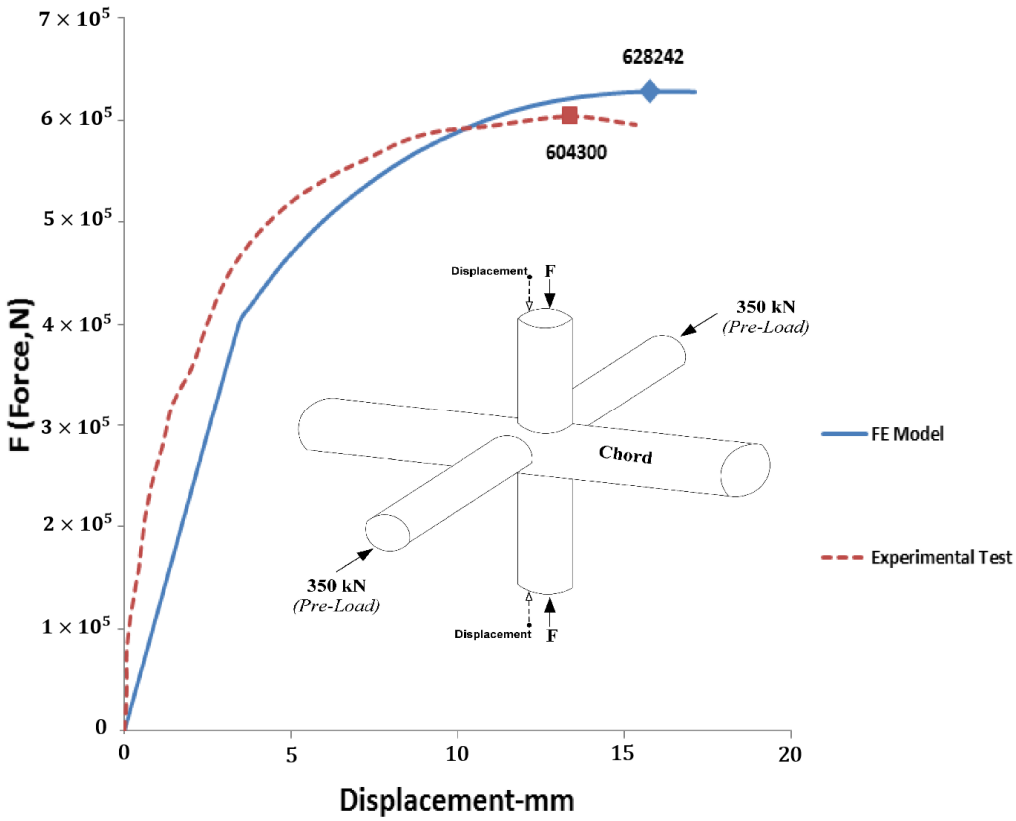

Figure 10: Finite element modeling result for 3-step loading test (ultímate strength) (Chiew *et al.* (1997)).

2.2.3 Corrosion modeling assumptions

As mentioned, there are different parameters for determining properties of a corroded region. In this study it is focused on two major parameters which are maximum depth of corrosion and corrosion distribution. The corrosion distribution is based on the average depth with standard deviation.

The data corresponding to these factors have been extracted and collected from sea filed. In order to study the effects of these two factors, three corrosion patterns have been used. The patterns are described in the following.

It should be noted that the starting time of corrosion is of important issue. It is assumed that corrosion begins in a range between 1.5 to 10 years after exposure to sea environment. According to research conducted by Guedes Soares and Garbatov (1999), corrosion starts a few years after the installation of structures in the environment and before that there is no significant corrosion (Emi *et al.* (1993), Loseth *et al.* (1994) and Guedes Soares and Garbatov (1999)). In this study, this time has not been considered wherever the age issue has been raised.

According to studies carried out, for routine inspections in the Persian Gulf, maximum corrosion depth of tubular members is reported as the critical corrosion parameter (Figure 11) (Iranian Offshore Oil Company (2009)). So for more applicable research, models of corrosion include maximum corrosion depth. As seen in Figure 11, the critical areas are located in the vicinity of joints between braces and the main member.

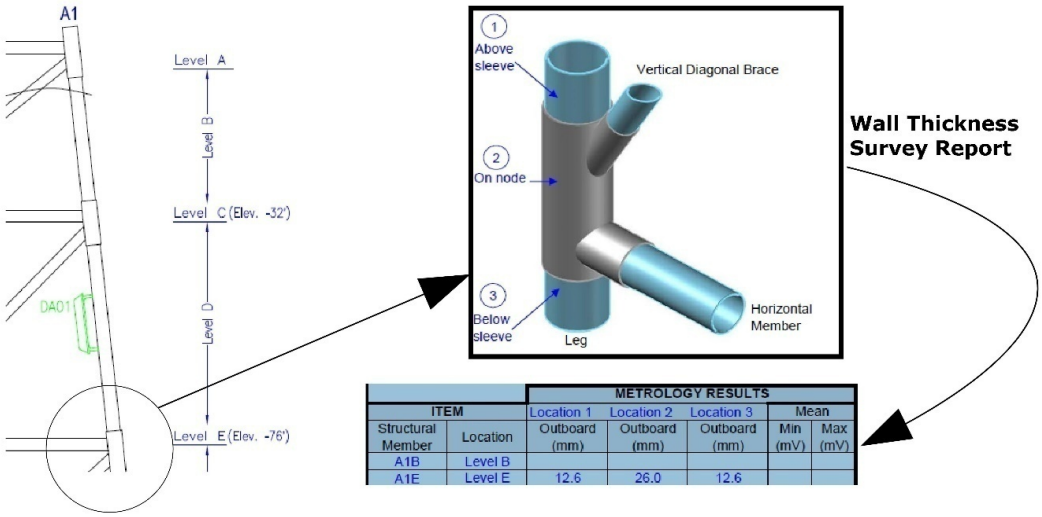

(a)

(b)

Figure 11: a) Routine inspection report of a platform in Persian Gulf b) A corroded member in Persian Gulf (Iranian Offshore Oil Company (2009)).

It should be noted that different annual corrosion rates have been expressed by researchers such as Qin and Cui (2003). Linear and nonlinear models are used to predict a corrosion wastage. In this study, a linear corrosion rate is used for the first and the second corrosion patterns; the third corrosion pattern is based on a nonlinear rate. In order to make an appropriate approximation of corrosion rates, two homogeneous series of data were extracted. The linear corrosion rate used in this study is based on values described in "Design method for steel structures in marine environment including the corrosion behavior (European Commission)". Table 3 presents maximum corrosion depth suggested by Houyoux and Alberts (2007).

Time (Year)	5	25	50	75	100
$Cr_{\max}$ (mm)	0.55	1.90	3.75	5.60	7.50

Table 3: Maximum of corrosion depth ($Cr_{\max}$) (Houyoux and Alberts (2007)).

Where Cr_{max} is maximum corrosion depth and Year represents age of corrosion in years.

According to Melchers-South well nonlinear formula, based on the average depth with standard deviation (Qin and Cui (2003)), main parameters are as follows:

$$Cr_{mean} = 0.084 Year^{0.823} \tag{1}$$

$$Cr_{SD} = 0.056 Year^{0.823} \tag{2}$$

The average depth (Cr_{mean}) and standard deviation (Cr_{SD}) area function of structure age in years.

2.2.4 Corrosion Applying

As mentioned above, corrosion can be categorized by its distribution on the surface of tubular members. In this study, two ways of applying general corrosion are used. Zone A and zone B represents these two ways. Zone A is defined across the length of member, while zone B represents corrosions with a length of more than twice the tube diameter and width of more than 30% of tube circumference (Figure 1).

It should be noted that for some models, corrosion is only applied on the main member. On the other hand, in models with corrosion on braces, all of four braces have corrosion on their surfaces. Also in models with zone “B" which is assumed as locally corroded region, this area has been chosen on the main member at the vicinity of the joint. This is because of stress concentration in this region and also the highest possibility of corrosion in the area. Figure 12 shows these two zones.

2.2.5 Corrosion Modeling Methods

In this study three methods of corrosion have been utilized. The characteristics of these models are based on maximum depth of corrosion and average corrosion depth with standard deviation.

2.2.5.1 First Corrosion Modeling Method

The first corrosion model has smooth reduction of thickness (Lutes *et al.* (2001)). As shown in Table 3 this reduction is modeled by maximum corrosion depth. Figure 13 shows numerical model of this type of corrosion.

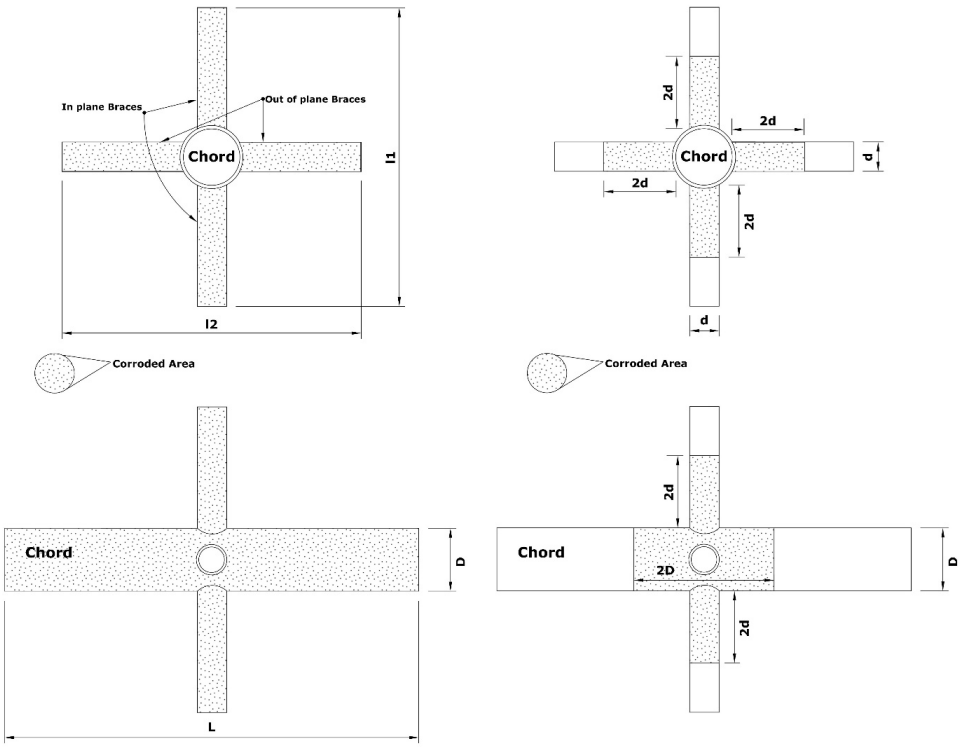

(a) (b)

Figure 12: a) Applied corrosion zone "A" b) Applied corrosion zone "B".

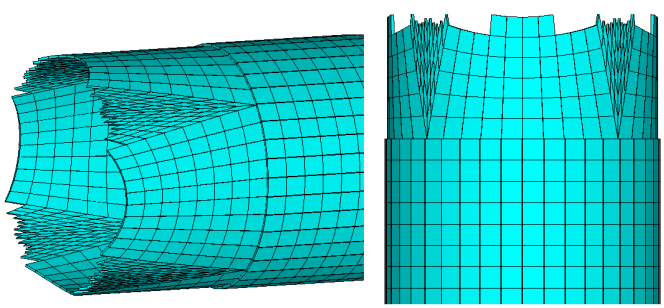

Figure 13: FE model of first corrosion modeling method applied on zone "B" forchord.

2.2.5.2 Second Corrosion Modeling Method

The second pattern of corrosion in the tubes is non-uniform. Non-uniform corrosion can be modeled in different ways. One sided asymmetric external corrosion is considered in this study which has been used by Lutes*et al.* (2001). The main characteristic ofthis type of corrosion is maximum depth of corrosion. According to equation (3) and Figure 14, the thickness of each section is defined as follows:

$$t\left(\theta_1\right) = t_0 - \frac{Cr_{max}\left|\theta_1\right|}{\pi}, -\pi \leq \theta_1 \leq \pi \tag{3}$$

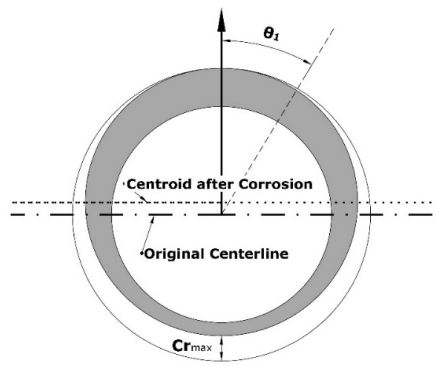

Figure 14: The cross section of a corroded tubular member with second corrosion pattern (one sided asymmetric external corrosión, Lutes *et al.* (2001)).

In this equation, $t\left(\theta_1\right)$ is the thickness of the section of the member at angle θ_1, and t_0 is the initial thickness of the tube. Also, thickness changes in the longitudinal direction of the member. Figure 15 shows cross sections of tube at different locations. As Figure 15 shows, the ratio of thickness change shows a sinusoidal pattern both in circumferential and longitudinal direction. As shown in Figure 15, two equally sized waves are formed along the corrode region. Figure 16 shows how the number of waves changes in a fixed-length. Figures 17 and 18 show numerical models with this type of corrosion.

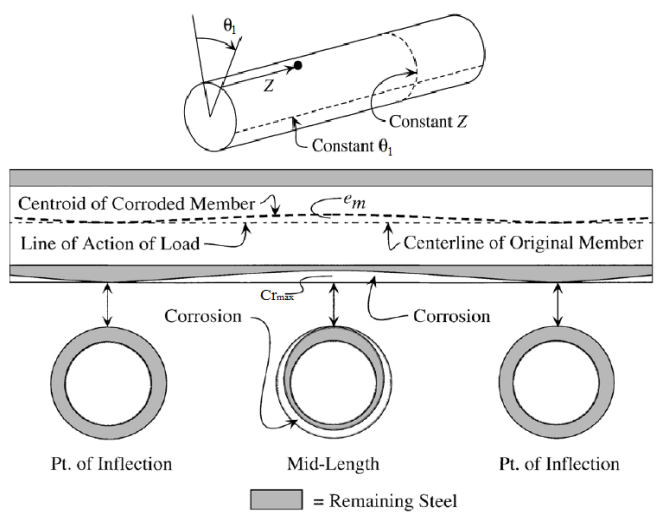

Figure 15: The cross sections of a corroded tubular member with second corrosion pattern (Lutes *et al.* (2001)).

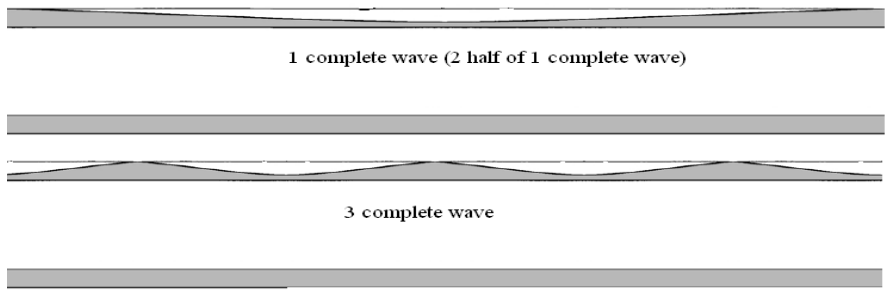

(a)

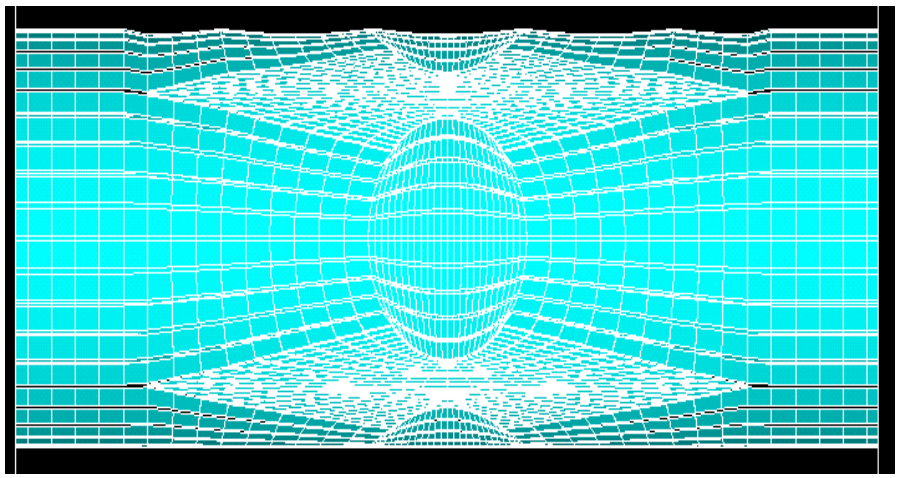

(b)

Figure 16: a) Schematic view of a corroded tubular member.
b) FE model with four waves in zone "B" (Lutes *et al.* (2001)).

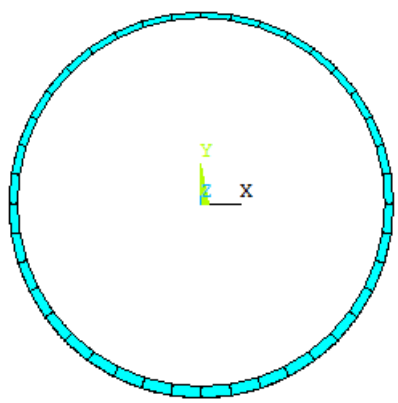

Figure 17: Cross section of FE model with one wave in zone "A" for chord (second corrosion type).

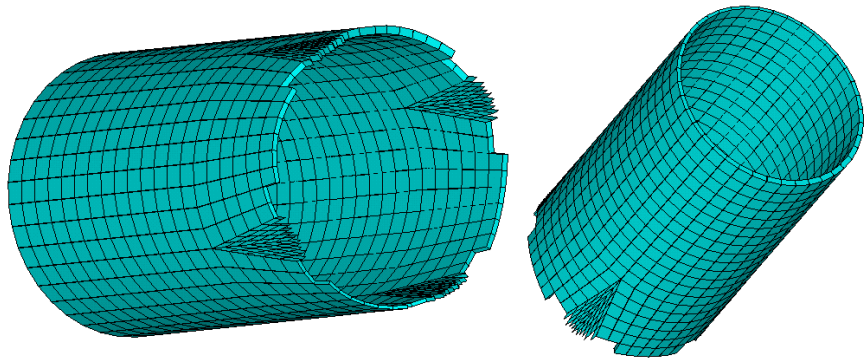

Figure 18: FE modelwithone wave in zone "A" forchord (second corrosion type).

2.2.5.3 Third Corrosion Modeling Method

This model is based on the average depth with standard deviation obtained from Melchers-South well formula by Melchers (1999) with a normal distribution (Wika (2012)). This model was only used for comparison with previous models. This model requires high density of meshing that increases the numbers of calculations. Therefore, only zone "B" in chord has finer mesh and corrosion applied in the same zone. Figure 19 shows a numerical mode of this type of corrosion.

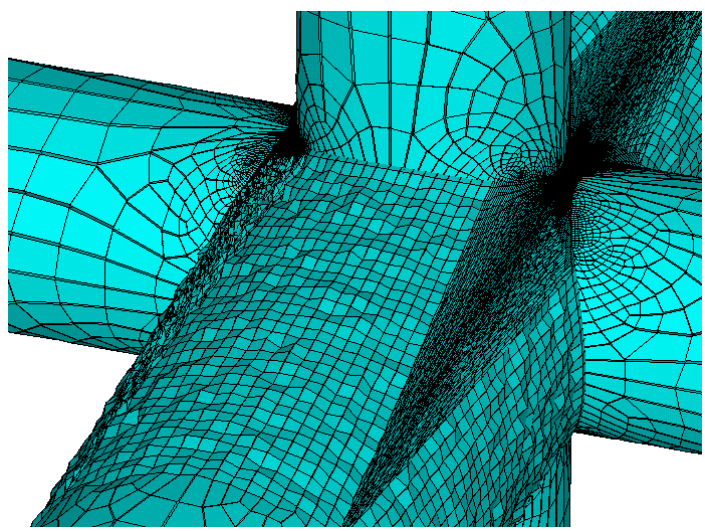

Figure 19: FE model of corrosión for zone "B" onchord surface (third corrosion type).

2.2.6 Meshing

The present numerical model and its meshing is based on studies of Chiew *et al.* (1999). In this study, maximum dimension of elements is assumed as a variable in order to optimize the numerical model and improve meshing quality. Also it is tried to make elements with equal sides. The elements become finer in the areas that braces join the chord (Figure 19). This plays an important role

in the convergence of the finite element solution. The sensitivity of analysis toward the size of elements was performed both for corroded and intact models. A numerical model for instance is comprised of 17000 elements.

2.2.6.1 Appropriate Meshing Density for Corrosion Modeling

The sensitivity analyses led to choose a meshing with maximum element size of 4 cm. In order to precisely model a corroded plate, it is necessary to use much smaller elements, i.e. 1 mm (Rahbar-Ranji (2012)). Of course for plates, the plate dimensions are not as large as a tubular joint and the type of corrosion modeling usually differs from the tubes. For modeling corrosion of tubes, elements with 2 mm dimension have been used (Yamane (2006)). But Saad-Eldeen *et al.* (2013) used elements of 5 cm dimension. Their study is close to this study in respect of structural aspects. Moreover, a sensitivity analysis was performed on a joint with Chiew *et al.* (1997) geometry tests in the zone "B". Then in the same zone, second corrosion modeling method was applied and the same analysis was performed. In two models, at the zone "B" and for the main member, the element dimensions have been reduced from 40 mm to 9 mm. As dimensions of elements decrease, the volume of numerical model and its processing time increase. The results of analyses are shown in figure 20.

In corroded model, the second type of corrosion was applied with one wave. Analysis was conducted with 40 mm elements and with the same corrosion at zone "B" with elements of 13 mm size.

Models with elements of 13 mm and 9 mm sizes showed no significant difference. As shown in Figure 20, these dimension changes have no clear change either with or without corrosion; therefore, 40 mm is a suitable dimension for elements.

3 RESULTS

In order to study the effects of geometry on strength of corroded joints, three different DX joints are modeled. The mechanical properties of these models are taken as same as joints of Chiew *et al.* (1997).Also the geometry of the models is equal to the experiments, e.g. the value ofαratio is selected in such a way to minimize the effects of boundary conditions on joint behavior. Table 4 presents dimensions of DX joints.

Then based on the corrosion modeling methods discussed earlier, joints with corrosion were modeled. The characteristics of corrosion are presented in Table 5. As mentioned earlier, in order to study effects of different parameters 75 models were analyzed in this study. These parameters include geometric, material properties and corrosion characteristics. Since the scope of this paper is to focus on effects of corrosion, the other models are not included. Also in order to emphasize the aims of the paper, the authors preferred to choose only 20 models. The ultimate strength of corroded models are compared with non-corroded models, i.e. Chiew *et al.* (1997) loading condition.

The ultimate strength of models are shown in tables 6. F_{Cor} indicates ultimate strength of the joint with corrosion. If $F_{Cor=0}$ is right, it means that there is no corrosion on the joint and d_{FE} represents joint displacement in ultimate state. Models 6, 9 and 10 represent joints of DX6, DX9 and DX10 without corrosion. In this study, it is assumed that a joint failure occurs when its main member fails (Figure 21).

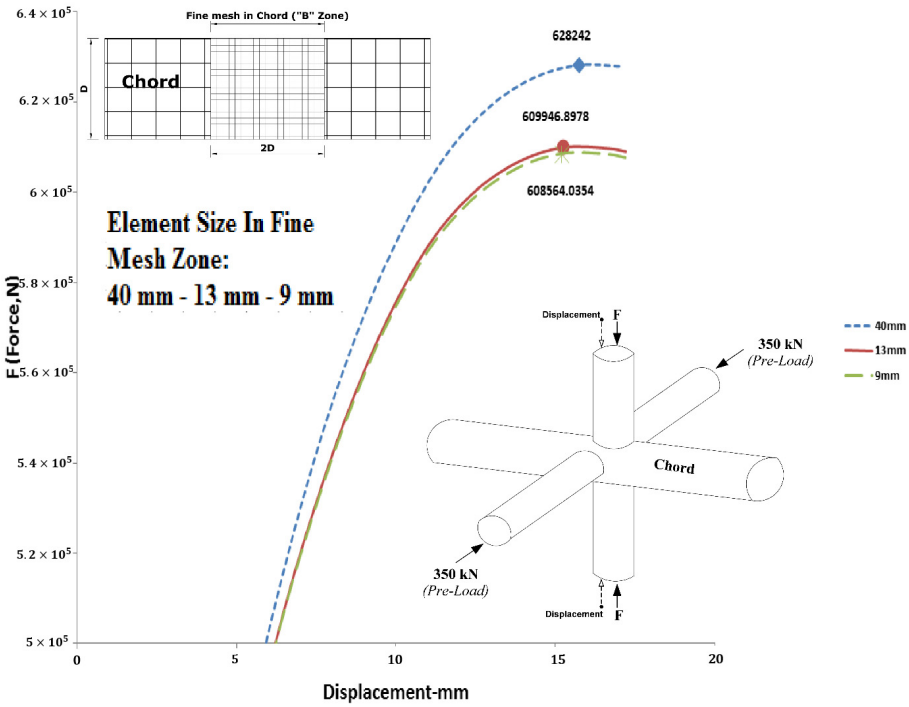

(a)

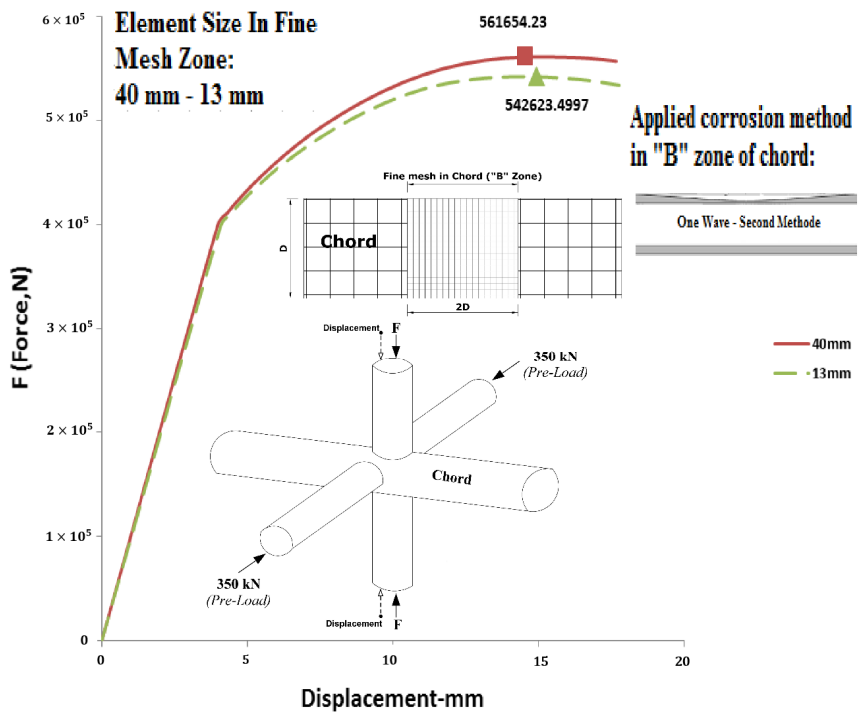

(b)

Figure 20: Sensitivity analysis a) non-corroded joint b) Corroded joint.

JointName	D(mm)	d(mm)	L(mm)	T(mm)	t(mm)	ϑ	l2(mm)	l1(mm)	β	τ	γ
DX6	500	300	5465	12	5	90	3122	2994	0.600	0.416	20.83
DX9	500	300	5465	12	10	90	3122	2994	0.600	0.833	20.83
DX10	500	300	5465	12	12	90	3122	2994	0.600	1	20.83

Table 4: Dimensions of joints DX6, DX9 and DX10.

Model Number	Geometrical Properties	Purpose	Preloading (kN)	Age of Corrosion (Year)	Corrosion in Chord		Corrosion in Braces		Corrosion Properties (mm)			Description
					Zone	Model	Zone	Model	Cr_{max}	Cr_{mean}	Cr_{SD}	
59	DX9	Wave Num. Effect in 2nd corrosión modeling method	320	25	B	2nd			1.9			With One Wave
60	DX9			25	B	2nd			1.9			With Two Waves
61	DX9			25	B	2nd			1.9			With Four Waves
21	DX6	Effect of Corrosion in Braces	320	25	A	2nd	A	2nd	1.9			With One Wave
25	DX10			25	A	2nd	A	2nd	1.9			With One Wave
36	DX6			25	A	1st	A	1st	1.9			
40	DX10			25	A	1st	A	1st	1.9			
66	DX6			25	A	2nd			1.9			With One Wave

Table 5: Characteristics of numerical models with the effects of corrosion. (continued).

(continuation)

Model Number	Geometrical Properties	Purpose	Preloading (kN)	Age of Corrosion (Year)	Corrosion in Chord		Corrosion in Braces		Corrosion Properties (mm)			Description
					Zone	Model	Zone	Model	Cr_{max}	Cr_{mean}	Cr_{SD}	
67	DX6	Effect of Corrosion in Braces	320	25	A	1st			1.9			
68	DX10			25	A	2nd			1.9			With One Wave
69	DX10			25	A	1st			1.9			
70	DX10	Comparing 3rd corrosion modeling method with 1st& 2nd	320	25	B	1st			1.9			
71	DX10			25	B	2nd			1.9			With One Wave
72	DX10			25	B	3nd				1.188	0.792	
73	DX10			5	B	1st			0.55			
74	DX10			5	B	2nd			0.55			With One Wave
75	DX10			5	B	3nd				0.3158	0.211	

Table 5: Characteristics of numerical models with the effects of corrosion.

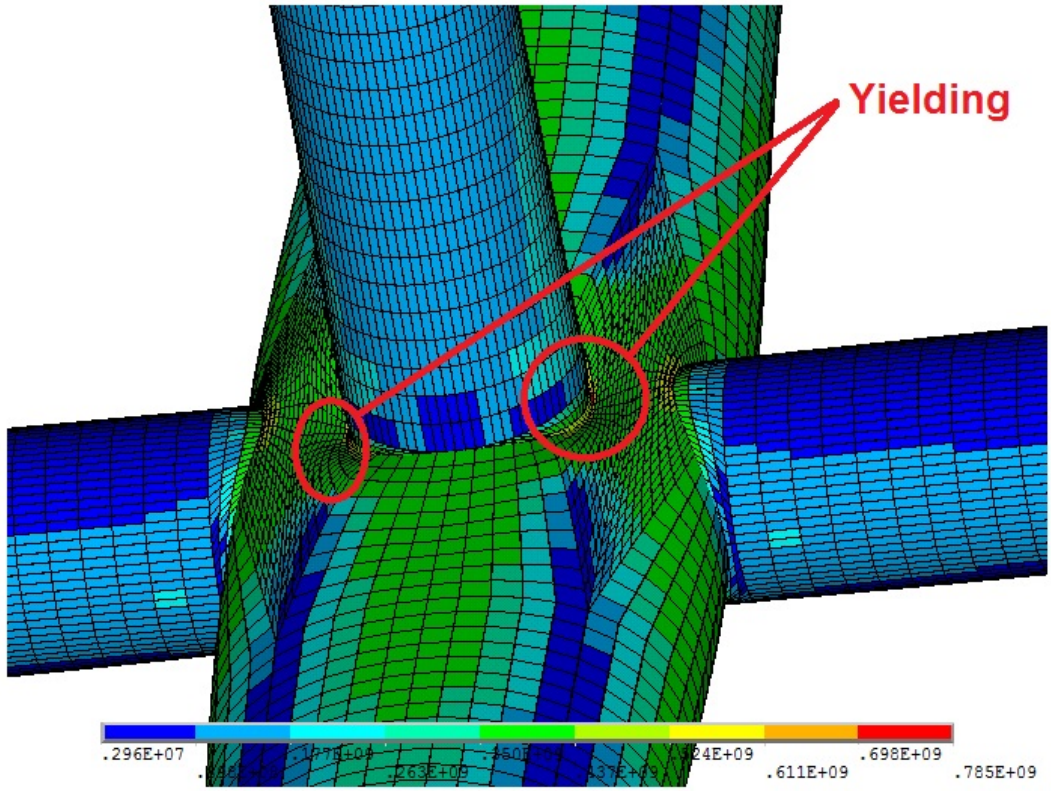

Figure 21: Stress distribution and deformation of DX6 joint at the ultimate strength state.

Model Number	$F_{Cor=0}$ Or F_{Cor} (kN)	d_{FE} (mm)	Model Number	$F_{Cor=0}$ Or F_{Cor} (kN)	d_{FE} (mm)
6	920.6976	17	66	817.8579	17
9	935.2138	18	67	710.4593	17
10	925.3163	18	68	800.5501	17
59	837.4587	15	69	712.7219	18
60	847.6352	16	70	755.7378	16
61	861.2652	16	71	832.8621	15
21	817.884	17	72	828.3735	16
25	799.9786	16	73	867.2978	15
36	691.4704	18	74	896.9807	15
40	711.1212	17	75	882.5071	15

Table 6: Ultimate strength and compression of braces (d_{FE}) using FEM.

The models 6, 9 and 10 are intact joints and have no corrosion. The reduction of ultimate strength for the remaining 17 models can be obtained using table 6.

The first pattern is a common way of modeling corrosion defects. Joints with this kind of corrosion demonstrate the lowest level of strength. e.g. the strength of models 36 and 40 is reduced by 25% and 23.2% respectively; while for the joints with the same conditions, but with the second corrosion pattern, i.e. models 21 and 25, reductions of 11.2% and 13.5% are observed.

The joints 59, 60 and 61 have corrosion defects based on the second pattern. As it is presented in table 6, an increase in the number of waves from 1 to 4, causes a reduction of about 2.5% in ultimate strength.

Also, the strength of a corroded joint depends on location of damaged area. As it is shown in the table 6, one can say that tubular DX joints with the first and second patterns of corrosion show similar behaviors in relation to location of damaged area. According to models 68 to 71, it is found that for the first pattern, 6% of strength drop occurs for the joint with corrosion at zone A compared to the joint with corrosion at zone B. This difference is expected to be 4% for the second pattern corrosion. In the next sections, these strength reductions discussed.

3.1 Effect of Number of Corrosion Waves

Figure 22 shows effect of number of corrosion waves on ultimate strength of DX joints. One can say that for joints with second corrosion pattern, as the number of waves increases, the ultimate strength of joints increases.

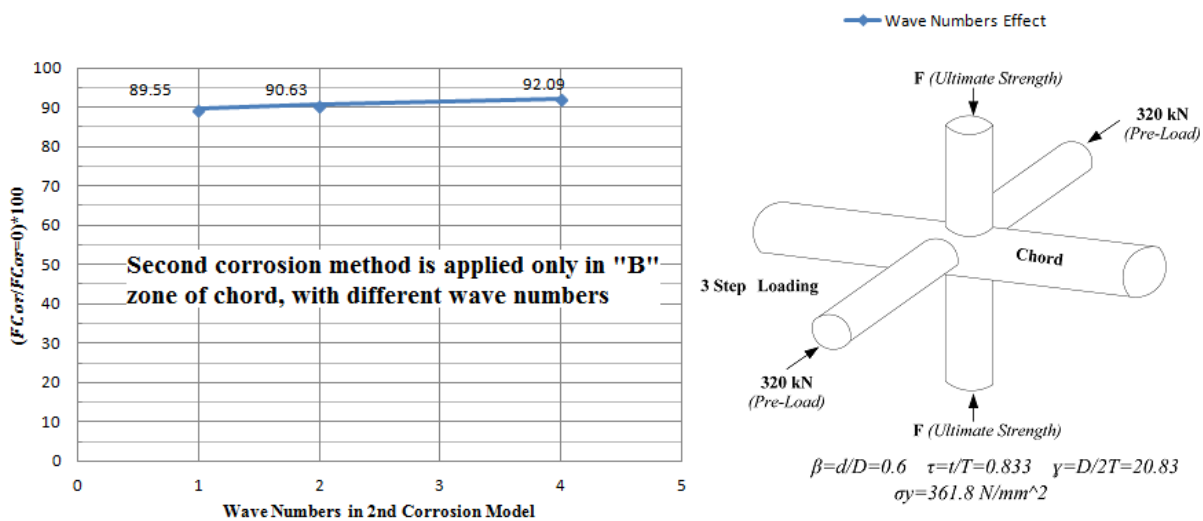

Figure 22: Effect of wave number on ultímate strength of joints with second corrosión pattern.

3.2 Behavior of Joints with Corroded Braces

Table 7 presents ultimate strength of joints affected by the first and second corrosion patterns. In some cases, the corrosion may cause the braces to be exposed to the risk of being failed.

Mod-el-Number	Geometrical Properties	Corrosion Model	Corrosion Zone	F_{Cor} *(kN)*	Diffrenc with Non-Corrode Model (%)	Diffrence of Non-Corroded brace Model With Corroded One
67	DX6	1st	A (Non-Corroded Braces)	710.4593	22.83	2.67
36		1st	A (Corroded Braces)	691.4704	24.9	
66		2nd	A (Non-Corroded Braces)	817.8579	11.17	0.003
21		2nd	A (Corroded Braces)	817.884	11.17	
69	DX10	1st	A (Non-Corroded Braces)	712.7219	23.22	0.22
40		1st	A (Corroded Braces)	711.1212	25.27	
68		2nd	A (Non-Corroded Braces)	800.5501	11.61	0.07
25		2nd	A (Corroded Braces)	799.9786	11.61	

Table 7: Effect of corrosion in braces.

3.3 Comparison of the Three Corrosion Patterns

Table 8 shows that the third corrosion pattern matches well with the second pattern. This corrosion model is more detailed and adapted to reality. It is also comprised of more elements that causes a time consuming process. Therefore, the second model is a suitable corrosion pattern to be studied in this paper.

Model Num-ber	Geometrical Proper-ties	Corrosion Model	Corrosion Age (Year)	F_{Cor} (kN)	Diffrence of 3rd Model with 1st Model (%)	Diffrence of 3rd Model With 2nd Model (%)
70	DX10	1st	5	755.7378	8.77	0.54
71		2nd	5	832.8621		
72		3rd	5	828.3735		
73	DX10	1st	25	867.2978	1.75	1.64
74		2nd	25	896.9807		
75		3rd	25	882.5071		

Table 8: Comparing the three corrosión modeling methods.

4 CONCLUSIONS

A numerical study on ultimate strength of 20DX tubular joints with corrosion defects was conducted. Three different corrosion patterns were discussed, and reduction of ultimate strength in terms of corrosion characteristics was presented. The effects of these three corrosion patterns were also compared with each other.

A sensitivity analysis was performed in order to achieve a balance between mesh sizing and accuracy of the results. The optimum element sizes were selected regarding dimensions of joint and corroded area.

The first corrosion pattern was modeled as a uniform reduction of wall thickness in a confined region. This pattern was based on linear relation of corrosion depth and time. Empirical equations were used to predict material loss in terms of time. Then the ultimate strength of the joints was obtained as a function of structure age. Due to higher material loss, joints with the first corrosion pattern showed more reduction of ultimate strength than ones with the other two patterns. This implies that common ways of corrosion modeling are very conservative.

The non-uniform material loss of joints with the second pattern was modeled by sinusoidal forms over tubular surfaces. The relation between decrease in joint strength and number of sinusoidal waves of corrosion was studied. It was shown that an increase in the number of waves causes a reduction in effects of corrosion.

In order to predict corrosion characteristics of the third pattern, a nonlinear criterion was used. The average corrosion depth and standard deviation of thickness were chosen for random distribution of thickness over the surfaces.

Also it was found that the effects of corrosion reduce in cases where corrosion occurs on brace surface. However, for joints with the first corrosion pattern, as the ratio of the maximum depth of corrosion to the initial thickness increases, braces become vulnerable to failure.

The importance of affected zone location was also investigated. The analyses demonstrated that thickness changes of the chord on the vicinity of joints play an important role on ultimate strength. In the other words, the surface of the chord member at the intersection of braces is of great significance and special attention should be paid for corrosion protection of this area.

References

ANSYS 14.0 reference manual (2012). ANSYS Inc.

Boone, T. J., Yura, J. A., Hoadley, P. W. (1982). Chord stress effects on the ultimate strength of tubular joints, P. M. Furguson Struct. Eng. Lab Rep. 82-1, Univ. of Texas at Austin, Austin, Tex., USA.

Chamberlain, J. (1988). Corrosion for students of science and engineering, Longman Scientific & Technical.

Chen, Y., Feng, R., Xiong, L. (2016). Experimental and numerical investigations on double-skin CHS tubular X-joints under axial compression. Thin-Walled Structures, 106: 268-283.

Chiew, S.P., Soh, C.K., Fung, T. C. (1997). Large Scale Testing of a Multiplanar Tubular DX-Joint. Proceedings of the Seventh International Offshore and Polar Engineering Conference Honolulu, USA.

Chiew, S.P., Soh, C.K., Fung, T.C., Soh, A.K. (1999). Numerical study of multiplanar tubular DX-joints subject to axial loads. Computers and Structures, 72: 749-61.

Cosham, A., Hopkins, P., Macdonald, K.A. (2007). Best practice for the assessment of defects in pipelines– Corrosion. Engineering Failure Analysis 14: 1245–1265.

Dexter, E. M. (1996). Effects of overlap on behaviour and strength of steel circular hollow section joints, PhD thesis, University of Wales, Swansea, Wales.

Emi, H., Yuasa, M., Kumano, A., Arima, T., Yamamoto, N., Umino, M. (1993). A study on life assessment of ships and offshore structures (3rd report: corrosion control and condition evaluation for a long life service of the ship). J Soc Nav Archit Jpn, 174: 735-744.

Gho, W.M., Gao, F., Yang, Y. (2006). Strain and stress concentration of completely overlapped tubular CHS joints under basic loadings. Journal of Constructional Steel Research, 62: 656–674.

Gho, W.M., Yang, Y., Gao, F. (2006). Failure mechanisms of tubular CHS joints with complete overlap of braces. Thin-Walled Structures, 44: 655–666.

Guedes Soares, C., Garbatov, Y. (1999). Reliability of maintained, corrosion protected plates subjected to nonlinear corrosion and compressive loads. Marine Structures, 12: 425-445.

Hairil Mohd, M., Paik, J.K. (2013). Investigation of the corrosion progress characteristics of offshore subsea oil well tubes. Corrosion Science, 67: 130-141.

Houyoux, C., Alberts, D. (2007). Design method for steel structures in marine environment including the corrosion behavior (European Commission), Vol. 1, First Edition, RFCS publications.

Iranian Offshore Oil Company (2009). Final report jacket inspection (Aboozar Field), Report No: 09/11/245.

Kang, C. T., Moffat, D. G., Mistry, J. (1998). Strength of DT tubular joints with brace and chord compression. Journal of Structural Engineering, 124: 775-783.

Khedmati, M.R. (2000). Ultimate strength of ship structural members and systems considering local pressure loads, Dr Eng thesis, Graduate School of Engineering, Hiroshima University, Japan.

Lan, X., Wang, F., Ning, C., Xu, X., Pan, X., Luo, Z. (2016). Strength of internally ring-stiffened tubular DT-joints subjected to brace axial loading. Journal of Constructional Steel Research, 125: 88-94.

Lee, M. M. K., Llewelyn-Parry, A. (2005). Strength prediction for ring-stiffened DT-joints in offshore jacket structures. Engineering Structures 27: 421–430.

Lee, M. M. K., Wilmshurst, S. R. (1996). A parametric study of strength of tubular multiplanar KK-joints. Journal of Structural Engineering, 122: 893–904.

Lee, M. M. K., Wilmshurst, S.R. (1997). Strength of multiplanar KK-joint under anti symmetrical loading. Journal of Structural Engineering, 123: 755–64.

Lesani, M., Bahaari, M. R., Shokrieh, M. M. (2013). Detail investigation on un-stiffened T/Y tubular joints behavior under axial compressive loads. Journal of Constructional Steel Research, 80: 91-99.

Loseth, R., Sekkeseter, G., Valsgard, S. (1994). Economics of high tensile steel in ship hulls. Marine Structures, 23: 31-50.

Lutes, L. D., Kohutek, T.L., Ellison, B.K., Konen, K.F. (2001). Assessing the compressive strength of corroded tubular member. Applied Ocean Research, 23: 263-268.

Makelainen, P. K., Puthli, R. S. (1988). Semi-analytical models for the static behavior of T and DT Tubular joints. International Conference on Behaviour of Offshore Structures (BOSS), Trondheim, Norway, 1285-1300.

Marshall, P. W., Toprac, A. A. (1974). Basis for tubular joint design. Welding Journal, 53: 192-201.

Miki, C., Kobayashi, T., Oguchi, N., Uchida, T. (2000). Deformation and fracture properties of steel pipe bend with internal pressure subjected to in-plane bending, WCEE.

Moffat, D. G., Kruzelecki, J., Blachut, J. (1994). Static strength of T and DT tubular joints in offshore structures, Rep. No. A/169194, University of Liverpool, Liverpool, U.K.

Nassiraei, H., Lotfollahi-Yaghin, M. A., Ahmadi, H. (2016). Static strength of collar plate reinforced tubular T/Y-joints under brace compressive loading. Journal of Constructional Steel Research, 119: 39-49.

Nassiraei, H., Lotfollahi-Yaghin, M. A., Ahmadi, H. (2016). Static strength of doubler plate reinforced tubular T/Y-joints subjected to brace compressive loading: Study of geometrical effects and parametric formulation. Thin-Walled Structures, 107: 231-247.

Paul, J. C. (1992). The ultimate behavior of multiplannar TT-and KK-Joints made of circular hollow sections, PhD thesis, Kumamoto University, Kumamoto, Japan.

Qin, S., Cui, W. (2003). Effect of corrosion models on the time-dependent reliability of steel plated elements. Marine Structures, 16:15-34.

Rahbar-Ranji, A. (2012). Ultimate strength of corroded steel plates with irregular surfaces under in-plane compression. Ocean Eng., 54: 261-269.

Saad-Eldeen, S., Garbatov, Y., Guedes Soares, C. (2013). Ultimate strength assessment of corroded box girders. Ocean Eng, 58: 35-47.

Togo, T. (1967). Experimental study on mechanical behaviour of tubular joints, PhD dissertation, Osaka Univ., Osaka, Japan.

UEG offshore Research (1985). Design of tubular joints for offshore structures Vol.3, UEG offshore Research.

van der Vegte, G.J., de Koning, C.H.M., Puthli, R.S., Wardenier, J. (1991). The Static Strength and Stiffness of Multiplanar Tubular Steel X-Joint. International Journal of Offshore and Polar Engineering, 1: 42-52.

Washio, K., Togo, T., Matsui, Y. (1968). Experimental studies on local failure of chords in tubular truss joints: Part I, Technol. Rep., Osaka Univ., Osaka, Japan.

Washio, K., Togo, T., Matsui, Y. (1969). Experimental studies on local failure of chords in tubular truss joints: Part II., Technol. Rep., Osaka Univ., Osaka, Japan.

Wika, S.F. (2012). Pitting and Crevice Corrosion of Stainless Steel under Offshore Conditions, Msc Thesis, Norwegian University of Science and Technology, Trondheim, Norway.

Yamane, M. (2006). Residual Strength Evaluation of Corroded Steel Members in Marine Environments. Proceedings of the Sixteenth International Offshore and Polar Engineering Conference, 43-50.

Yang, J., Shao, Y., Chen, C. (2012). Static strength of chord reinforced tubular Y-joints under axial loading. Marine Structures, 29: 226-245.

Yura, J. A., Swenssen, K. D. (1987). Ultimate strength of double-tee tubular joints: interaction effects, P. M. Furguson Struct. Eng. Lab Rep. No. 87-9, Univ.of Texas at Austin, Austin, Tex, USA.